Available online at www.sciencedirect.com
ScienceDirect
Journal of the European Ceramic Society 27 (2007) 1–12
www.elsevier.com/locate/jeurceramsoc

A 3-balls-on-3-balls strength test for ceramic disks

T. Fett [a,1], G. Rizzi [a], E. Ernst [a], R. Müller [b], R. Oberacker [b,*]

[a] *Forschungszentrum Karlsruhe, Institut für Materialforschung II, Karlsruhe, Germany*
[b] *Universität Karlsruhe, Institut für Keramik im Maschinenbau, Karlsruhe, Germany*

Received 26 November 2005; received in revised form 24 January 2006; accepted 4 February 2006
Available online 17 April 2006

Abstract

In the usual tests to determine strength or lifetime under tension, bending or compression loading, the uniaxial stress state is present. However, in components very often multiaxial stresses occur. But also under uniaxial external loading, multiaxial stresses are possible, for instance, in notched components. Common tests are bending tests on thin circular disks.

Following the description of conventional tests, a recently developed test using three loading and three supporting balls shall be addressed. For this test, the maximum principal stresses and the biaxiality are determined for a wide range of geometries by using the finite element method. First experimental results carried out on glass and alumina are reported.

It was found that in all cases the results of the 3-balls-on-3-balls (3B3B) tests are slightly lower than the strengths obtained from the ball-on-3-balls (1B3B) tests. The main reason for this tendency is assumed to be the influence of the different effective surfaces involved in the two types of tests. The Weibull exponents *m* for these tests overlap within the 90% confidence intervals.
© 2006 Elsevier Ltd. All rights reserved.

Keyword: Ceramic disk; Testing; Mechanical properties; Strength tests

1. Introduction

Conventional strength tests describe the failure behaviour of materials under simple stress conditions, in most cases, uniaxial stresses. In practical applications, however, mechanical loading often leads to multiaxial stresses. Therefore, experimental methods were developed quite early to determine the strength and deformation behaviour under multiaxial stress conditions (for an overview see ref.[1]):

- Ring-on-ring test (with modifications)[2–8]
- Sphere-on-ring test[9–11]
- Ball-on-3-balls (1B3B) test[12–16]
- Brazilian disk test[17–25]
- Thermal shock test[26,27]
- Pressurised tube test[28–31]
- Torsion test

Most of these strength tests require high-quality specimen surfaces (except for the ball-on-3-balls and the thermal shock test). It is the aim of this report to analyse a simple multiaxial strength test that allows testing of specimens in the "as fired" state. First, the ring-on-ring test with modifications shall be illustrated in detail. Then, a new test with six balls shall be addressed.[32] The stress solution will be determined and first experimental results on alumina and glass will be given.

2. Biaxial bending tests on disks

The principle of the concentric ring-on-ring test is illustrated in Fig. 1a (see refs.[2–6]). A disk-shaped specimen is supported by a ring and loaded by a concentric ring of smaller diameter.

The ring-on-ring test has been used extensively for strength measurements of glass and has been standardised. Whereas bending bars exhibit additional flaws at the edges, which are generated by the machining process, the edges of a circular disk are nearly free of stress and will not contribute to failure. In the case of a large overhang also the hoop stresses can be responsible for failure outside the supporting ring.[8]

This test device results in a well-defined stress state within the inner ring only under ideal loading conditions. For this,

* Corresponding author.
E-mail address: rainer.oberacker@ikm.uni-karlsruhe.de (R. Oberacker).
[1] Now guest scientist at Universität Karlsruhe, Institut für Keramik im Maschinenbau, Karlsruhe, Germany.

0955-2219/$ – see front matter © 2006 Elsevier Ltd. All rights reserved.
doi:10.1016/j.jeurceramsoc.2006.02.033

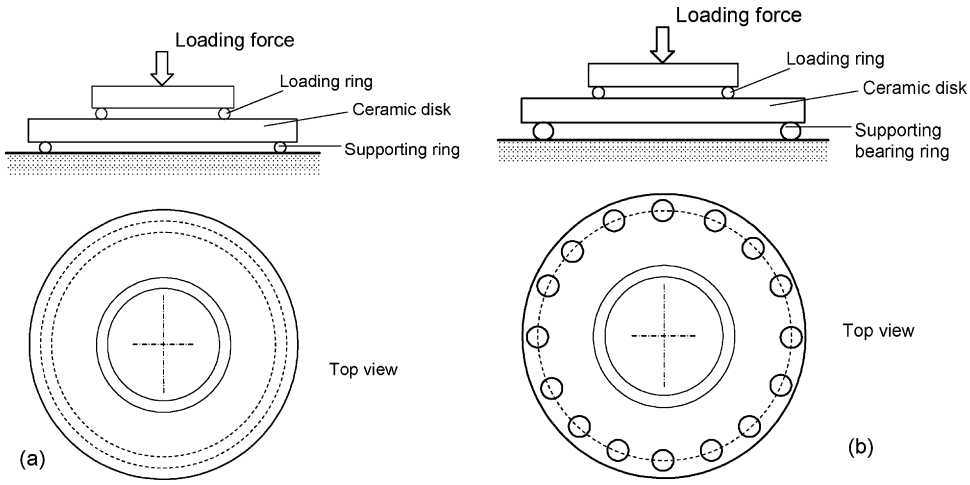

Fig. 1. (a) Ring-on-ring test, (b) ring-on-bearing ring test.

however, highly plane parallel disk-shaped specimens are required. If this is not the case, a three-point contact between ring and specimen will occur. Only at high loads will a continuous contact line develop, resulting in the correct stress distribution. In a modification of the ring-on-ring test, the supporting ring is replaced by a ball bearing ring (Fig. 1b). This ensures reduced friction between disk and supporting structure. Stress concentrations due to the Hertzian contacts are not of high importance, because the stresses superimposed by bending moments disappear in the supporting region. In a modification proposed by Marshall,[7] each ring consists of a linear spring with its ends joint to form a closely wound coil.

In order to avoid undefined supporting conditions, the ball-on-ring test was developed. In this test, a disk specimen is supported by a ring and loaded centrally with a ball (see Fig. 2). This test configuration was proposed by Shetty et al.[9,10] To reduce friction effects between disk and supporting ring, the latter is sometimes replaced by a ball bearing ring as used in Fig. 1b.

Another modification is the ball-on-3-balls configuration. Here, the outer ring is replaced by three balls. This results in statically well-defined conditions. This test is described in ref.[12]. Extensive computations of the stress state are given in ref.[13]. Errors resulting from misalignments and test specimen imperfections are discussed in ref.[14].

3. A new 3-balls-on-3-balls (3B3B) test

As already mentioned before, the ball-on-3-balls test yields statically well-defined mechanical boundary conditions. A disadvantage of this test configuration, however, is the relatively small effective surface tested. Due to the strongly decreasing stresses with increasing distance from the disk centre, the plate regions at larger distance hardly contribute to the failure behaviour.

This was the main reason why the test was modified[33] by reducing the influence of the point-like stress spots and significantly increasing the effective surface tested. As shown in Fig. 3, the outer supporting and the inner loading forces are applied by three spheres each. By this configuration, mechanically well-defined supporting conditions as well as well-defined loading conditions are achieved.

In Fig. 3a, the loading and supporting spheres are “in line“, i.e. the sphere centres are located at the same polar angle. Fig. 3b

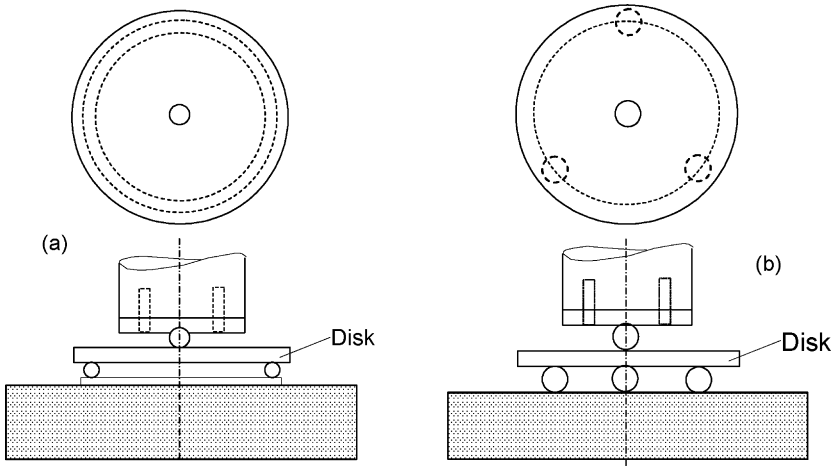

Fig. 2. (a) Ball-on-ring test, (b) ball-on-3-ball test.

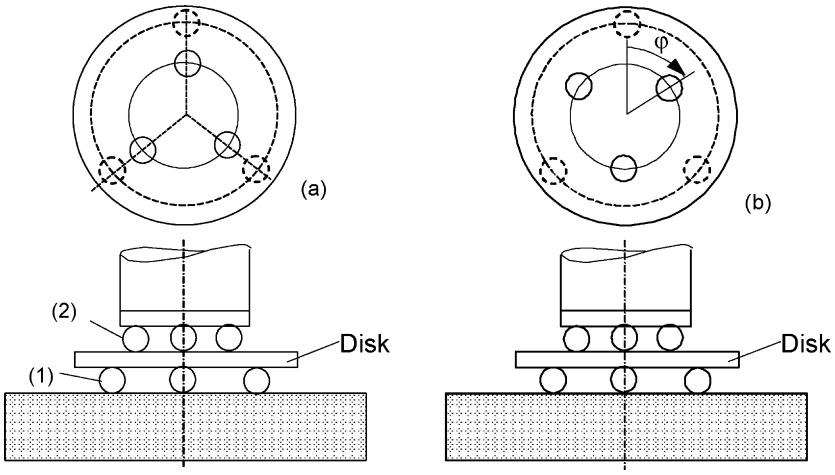

Fig. 3. 3-balls-on-3-balls test: (a) loading and supporting spheres in line, (b) loading and supporting spheres in line under an angle of $\varphi = 60°$.

shows the case of the inner and outer spheres being shifted by an angle of $\varphi = 60°$.

Fig. 4 gives a possible design. The loading (1) and supporting balls (2) are fixed in radial grooves (3) in the two metal plates (4, 5) with a small clearance in width direction. For the outer support rolls to move freely to outside during loading, they are pushed to the inner edge by soft springs (6) before the test. On the other hand, the inner loading spheres can move freely from the outer edge to the inside. Besides the spring solution represented in Fig. 4, also a magnet solution may be applied, as it is often done in bend tests. For this, the balls must be made of a magnetisable material (e.g. magnetisable steel).

The exact orientation of the two metal plates (4, 5) relative to each other and, hence, the exact location of the supporting and loading balls relative to each other is ensured by two metal pins (7) in the bore holes (8). These pins can be removed before load application in a testing machine.

4. Finite element computations

Fig. 5 shows the disk of radius R and the sphere location circles R_1 (loading spheres) and R_2 (supporting spheres). The ratio of outer to inner sphere circles was chosen to be $R_1/R_2 = 2$.

The finite element net is presented in Fig. 6. It may be used for considering the in line sphere application as well as 60° rotation of the inner spheres. In addition, the case of a "ball-on-3 balls" can be modelled. The disk was realised by a finite element net of about 24100 elements with 110400 nodes. The

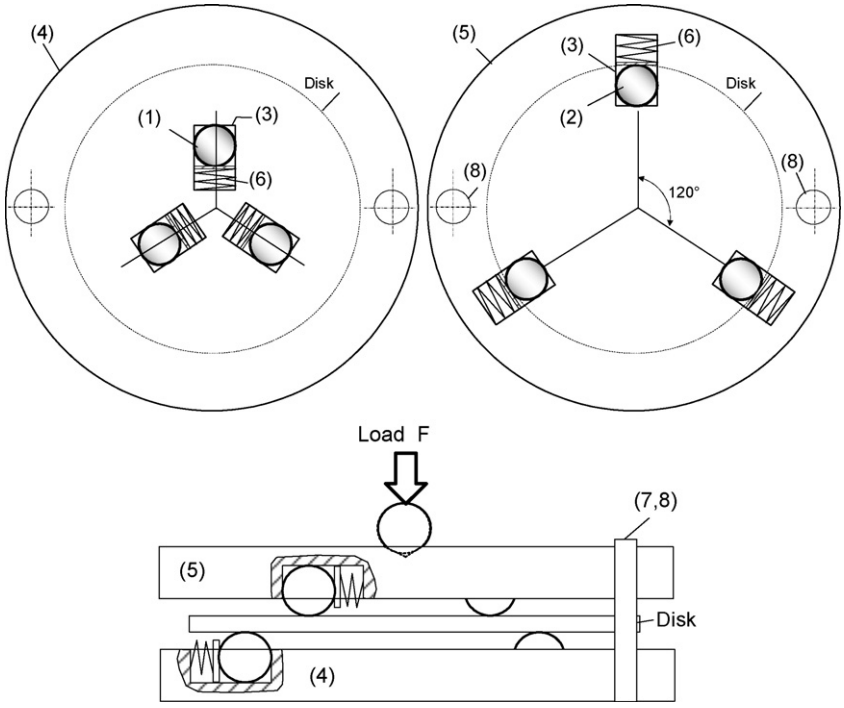

Fig. 4. A possible design for the test, including all degrees of freedom (free movement of the balls).

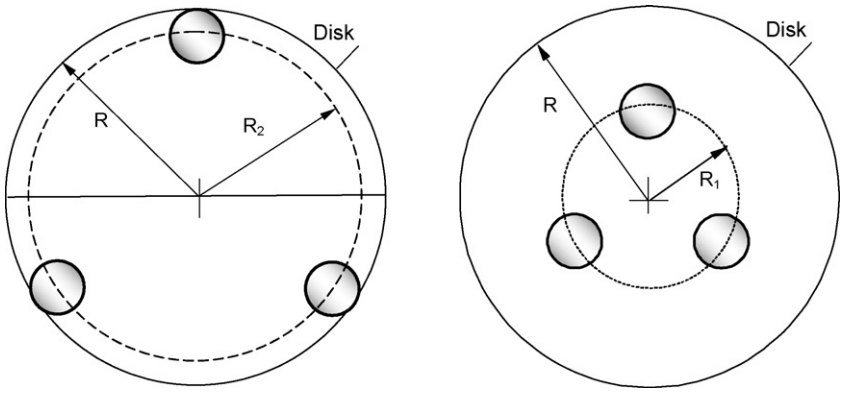

Fig. 5. Definition of the relevant radii R, R_1, and R_2.

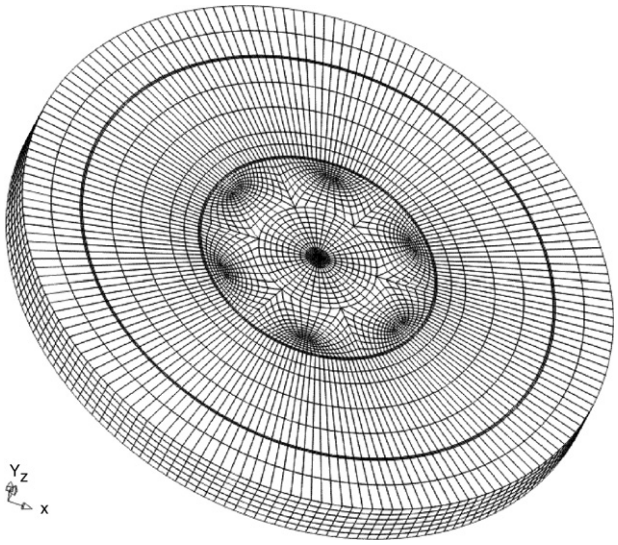

Fig. 6. Finite element net.

computations were carried out with ABAQUS version 6.3. For all FE computations, the radius of the circle on which the inner spheres are located was chosen arbitrarily as $R_1 = 1$.

The Theorem of Saint Venant ensures that no significant effect of the Hertzian contact radius a on the stresses can occur as long as a is clearly smaller than the plate thickness t. This condition is sufficiently satisfied for $a < t/3$. In this case only the resultant of the contact stresses (i.e. the total force) governs the stress in the surface underneath the loading balls. Under this condition also the shape of the pressure distribution over the contact area is without any importance.

A confirmation of this statement can be found in ref.[13]. In this paper it was shown in a detailed finite element study that in a wide range of contact radii not any influence on the maximum stress is detectable. Therefore, all our finite element results were obtained for an arbitrarily chosen contact radius of $a = 0.003\ R_1$ in which the load was applied by a constant pressure. It is furthermore, assumed that the spheres can freely move. Consequently, friction effects were neglected.

4.1. Loading and supporting balls in line

The maximum principal stress is represented in Fig. 7a for the thicknesses $t/R_1 = 0.1$ and $\nu = 0.25$. The stress levels are scaled according to $\sigma_1 t^2/F$.

Fig. 7b shows the ratio of the second (not disappearing) principal stress σ_2 to the maximum principal stress. It clearly indicates the biaxial stress state with a small variation in the central zone of the disk only. The value "1" represents an equibiaxial stress state. In this context, it should be noted that one of the principal stresses must disappear at the (free) disk surface.

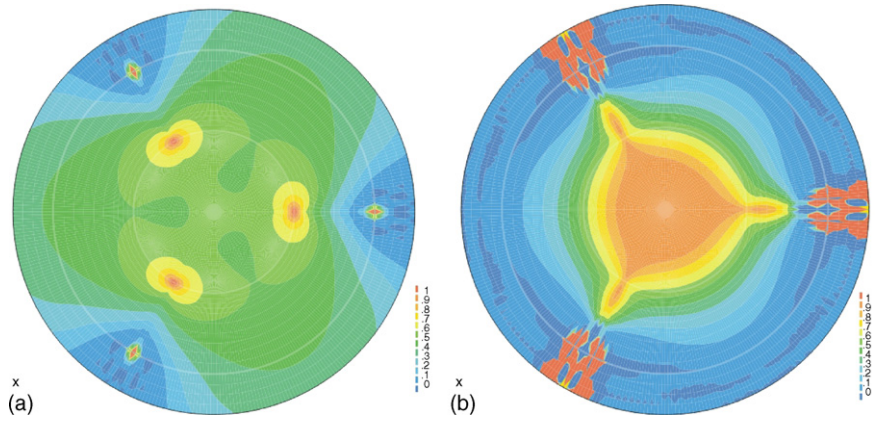

Fig. 7. (a) Maximum principal stress for a disk with $t/R_1 = 0.1$ and $\nu = 0.25$ (blue $\sigma_1 t^2/F = 0$, green = 0.5, red = 1), (b) stress biaxiality at the surface (blue $\sigma_2/\sigma_1 = 0$, green = 0.5, red = 1), $\varphi = 0$, $R/R_1 = 2.5$.

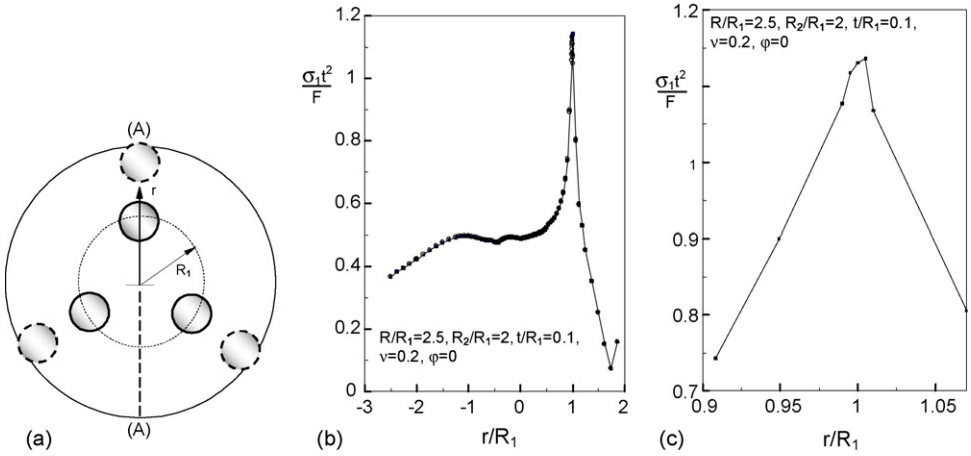

Fig. 8. Influence of the load application area on maximum principal stress, $\varphi = 0$.

Fig. 8b presents the maximum principal stress σ_1 over the cross section A–A (see Fig. 8a) with details near the inner sphere in Fig. 8c.

The influence of disk thickness t on the stresses is shown in Fig. 9. General proportionality $\sigma \propto 1/t^2$ can be concluded from the coincidence of the normalised stresses in the form of $\sigma t^2/F$ at larger distance from the contact zones. Fig. 10a and b show the effect of Poisson's ratio ν for $t/R_1 = 0.1$. The maximum principal stress increases slightly with increasing ν. Fig. 10c shows stresses for $t/R_1 = 0.4$.

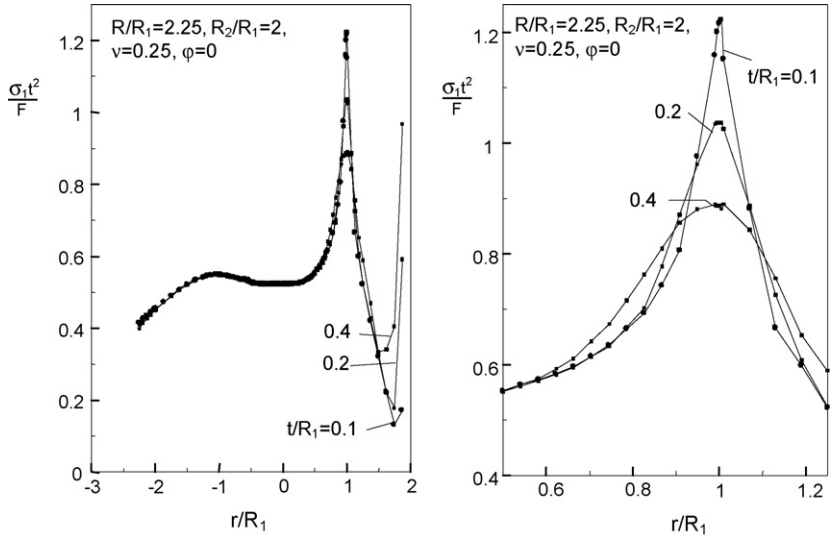

Fig. 9. Maximum principal stress: influence of specimen thickness.

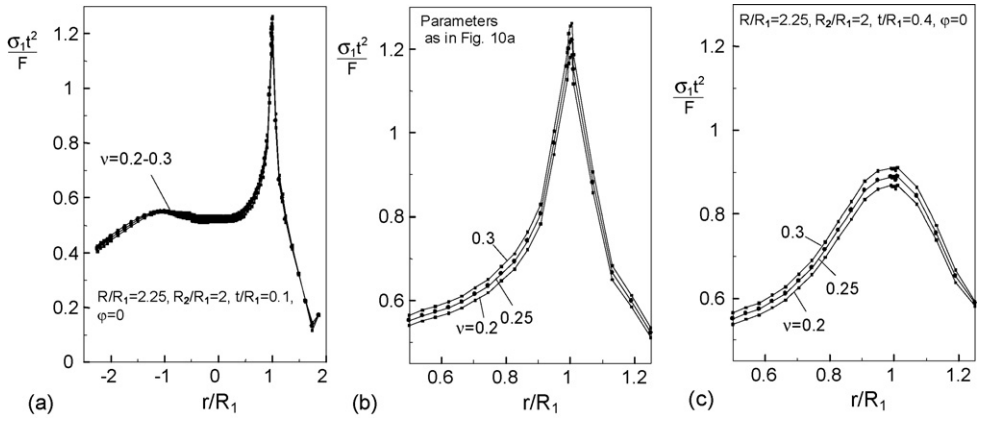

Fig. 10. Influence of Poisson's ratio on the maximum principal stress for $t/R_1 = 0.1$ and 0.4.

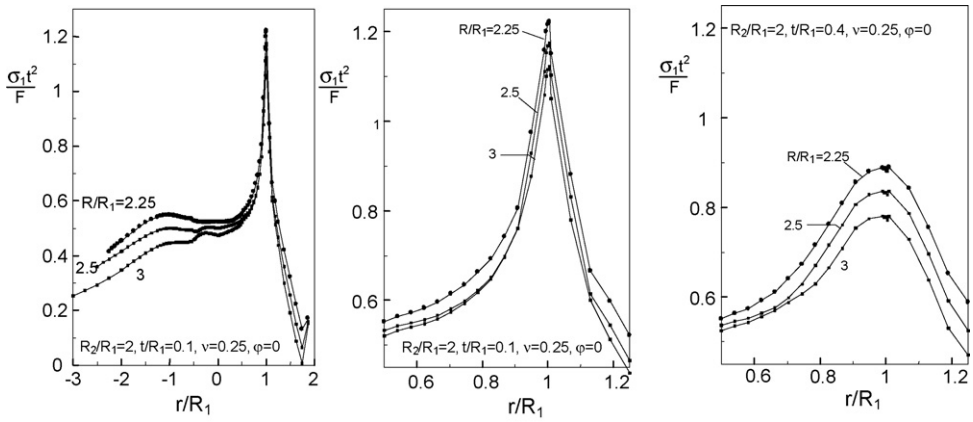

Fig. 11. Influence of the overhang on the maximum principal stress.

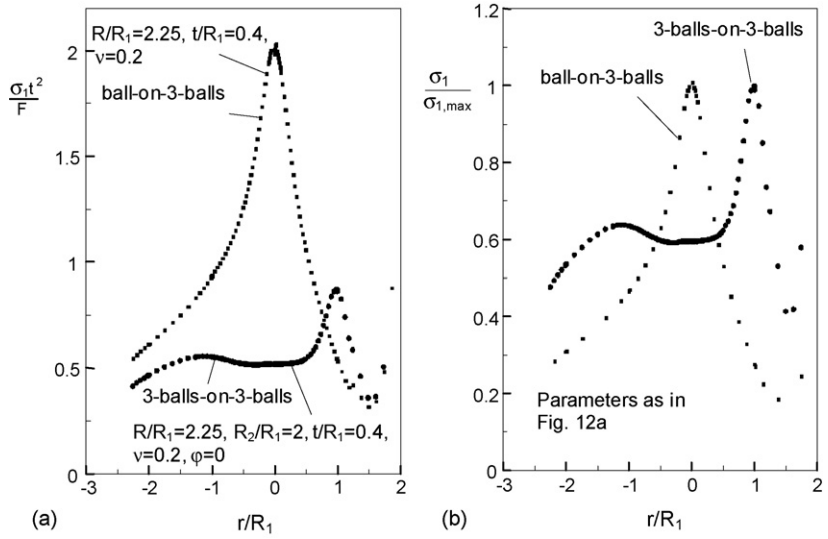

Fig. 12. (a) Maximum principal stress in a ball-on-3-balls test compared with the results of a 3-balls-on-3-balls test (balls in line), (b) normalised representation.

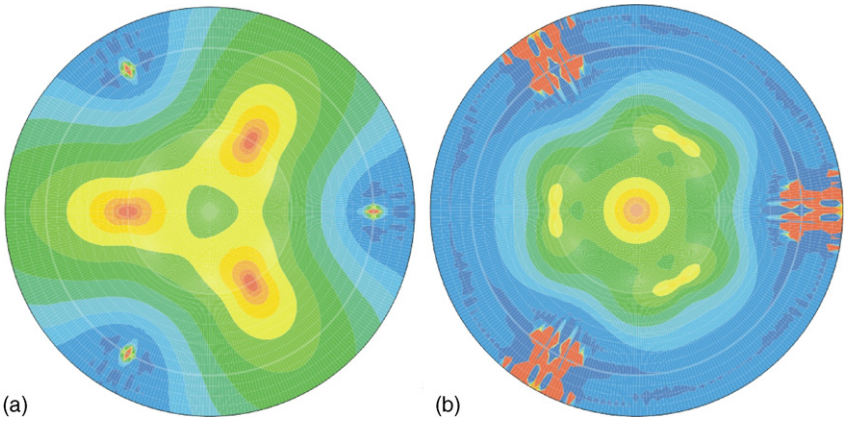

Fig. 13. a) Maximum principal stress for a disk of $t/R_1 = 0.1$ and $\nu = 0.25$ (blue $\sigma_1 t^2/F = 0$, green = 0.5, red = 1), (b) stress biaxiality at the surface (blue $\sigma_2/\sigma_1 = 0$, green = 0.5, red = 1), $\varphi = 60°$, $R/R_1 = 2.5$.

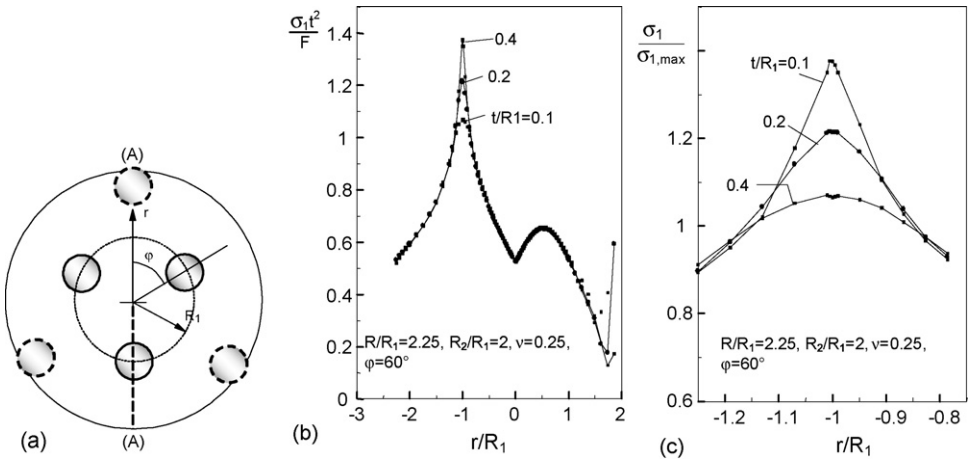

Fig. 14. Maximum principal stress along the line A–A for $\varphi = 60^\circ$: Influence of specimen thickness (at $r = 0$, an equibiaxial stress state occurs. Here, the stress component that defines the maximum principal stress changes).

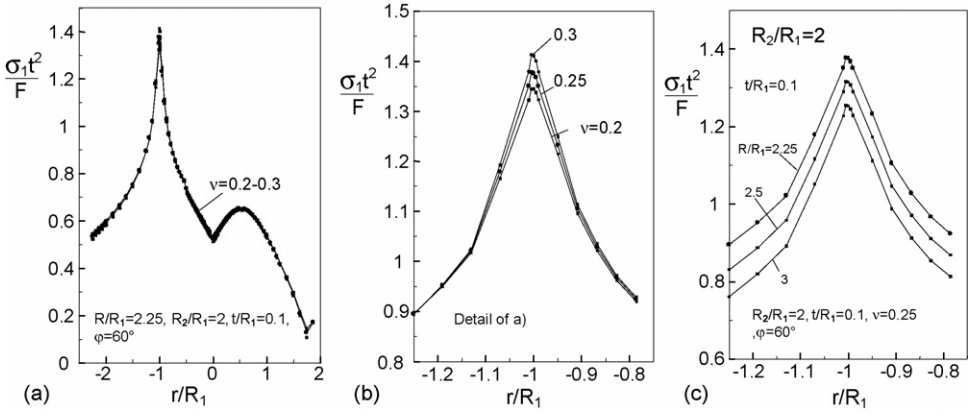

Fig. 15. Maximum principal stress: (a) and (b) influence of Poisson's ratio, (c) influence of the overhang, φ=60°.

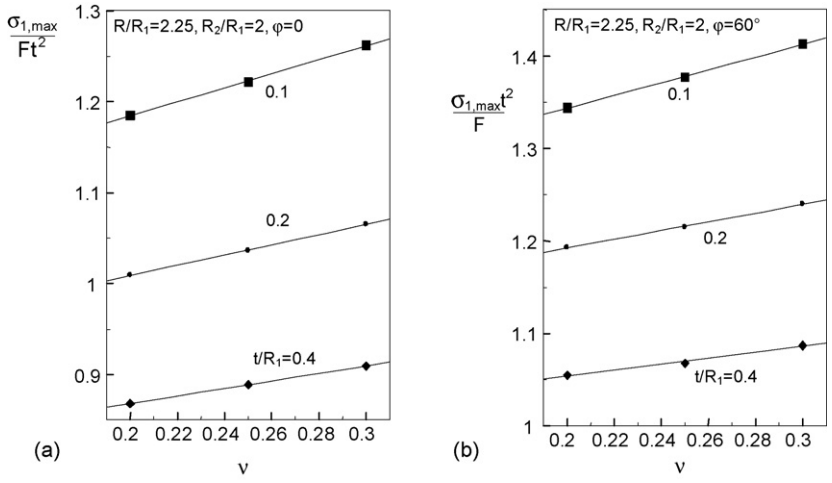

Fig. 16. Maximum values of the maximum principal stress as a function of Poisson's ratio ν (a) for $\varphi = 0$, (b) for $\varphi = 60^\circ$.

The disk radius R was varied within $2.25 \le R/R_1 \le 3$ defining the overhang. The influence of this parameter is visible from Fig. 11a–c.

4.2. Stresses for a ball-on-3-balls arrangement

The stress state of the ball-on-3-balls test was studied extensively by Börger et al.[13] Some own results are given in Fig. 12 for comparison of stresses and stress ratios with the results of a 3-balls-on-3-balls test.

From Fig. 12a, it can be concluded that the stresses in the 3-balls-on-3-balls test are significantly reduced compared to those occurring in the ball-on-3-balls test. The reason is that in the 3-balls-on-3-balls test total load is divided into three partial loads. More homogeneous stress distributions are obvious (Fig. 12b).

4.3. Loading and supporting balls under an angle of 60°

Figs. 13–15 represent the stresses in the case of the inner balls being rotated by 60°.

5. Conclusions from the computations

For the mostly recommended overhang of $R/R_1 = 2.25$, the final results are given in Fig. 16a for $\varphi = 0$ and Fig. 16b for $\varphi = 60°$.

For a disk with R/R_1=2.25, $0.1 \le t/R_1 \le 0.4$, and "sphere-in-line" conditions ($\varphi = 0$), the FE results can be expressed by

$$\sigma_{1,\max}\frac{t^2}{F} = 0.656\left(\frac{t}{R_1}\right)^{-0.196} + 0.274\left(\frac{t}{R_1}\right)^{-0.448}\nu \qquad (1)$$

For $\varphi = 60°$ and $R/R_1 = 2.25$, the maximum stress values can be approximated by

$$\sigma_{1,\max}\frac{t^2}{F} = 0.871\left(\frac{t}{R_1}\right)^{-0.142} + 0.197\left(\frac{t}{R_1}\right)^{-0.533}\nu \qquad (2)$$

6. Experimental results

First strength tests with disk-shaped specimens were carried out for two materials, a borosilicate glass (BK4, Schott, Mainz) with two different surfaces (a roughly ground surface with a roughness parameter $R_a = 0.36$ mμ and polished surfaces) and a fine-grained alumina (RK87, CeramTec, Plochingen) with a mean grain size of about 4 μm. The disk-shaped specimens were 45 mm in diameter with a thickness of 4 mm for the glass and 2 mm for the alumina. Twenty specimens each were tested in the ball-on-3-balls and the 3-balls-on-3-balls arrangements at $\varphi = 0°$ and $R_2/R_1 = 2$ (balls of a ball bearing of 8 mm in diameter). The strengths σ_c (defined as the maximum principle stress underneath the loading balls) were computed from the maximum load by Eq. (1) using $\nu = 0.22$ for glass and $\nu = 0.25$ for the alumina. Fig. 17 allows the strength for any R_2/R_1 and R/R_1 to be determined by interpolation. For the ball-on-3-balls tests, the strength was computed according to ref.[13].

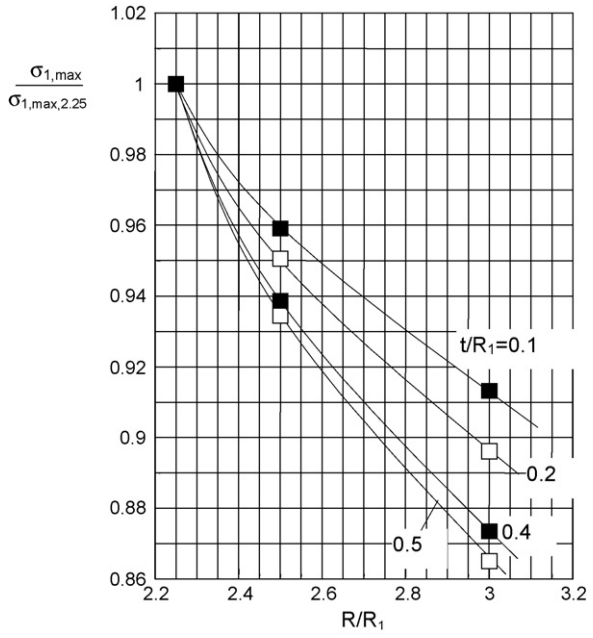

Fig. 17. Influence of the overhang on the maximum tensile stress (valid for $R_2/R_1 = 2$, $\varphi = 0$, and $0.2 < \nu \le 0.25$).

6.1. Results on glass

6.1.1. Ground glass

In a first series of 3-balls-on-3-balls tests, the outer radius R_2 was chosen to be $R_2 = 20$ mm. The strength results are shown in Fig. 18a as the circles. About 70% of the specimens failed in the centre region of the disk. These "regular results" are represented by the open circles. The rest of the specimens failed near the outer disk circumference (solid circles) where parts of the material chipped off. In order to avoid such an irregular fracture, the outer radius R_2 was reduced to $R_2 = 18$ mm ($R_1 = 9$ mm) in a second test series. The increased distance of now 4.5 mm from the outer sphere contact prevented any irregular failure. These results are represented by the squares in Fig. 18a. In Fig. 18b, these results (open squares) are compared with strength results obtained from ball-on-3-balls tests carried out with the supporting balls located on a circle of 20 mm radius (solid squares).

According to the relation for the failure probability F,

$$F(\sigma_c) = 1 - \exp\left[-\left(\frac{\sigma_c}{\sigma_0}\right)^m\right] \qquad (3)$$

the Weibull parameters for the strength m and σ_0 were determined with the "Maximum Likelihood Procedure" according to ref.[34]. The 90% confidence intervals were computed as suggested in ref.[35] and compiled in Table 1. The characteristic strength σ_0 of the ball-on-3-balls tests is slightly higher than that of the 3-balls-on-3-balls tests.

6.1.2. Polished glass

The strengths of polished glass disks are shown in Fig. 19a for the 3-balls-on-3-balls tests and ball-on-ball tests. The resulting Weibull parameters are compiled in Table 2. Also for this surface state the 3-balls-on-3-balls tests show lower strength than the ball-on-ball tests.

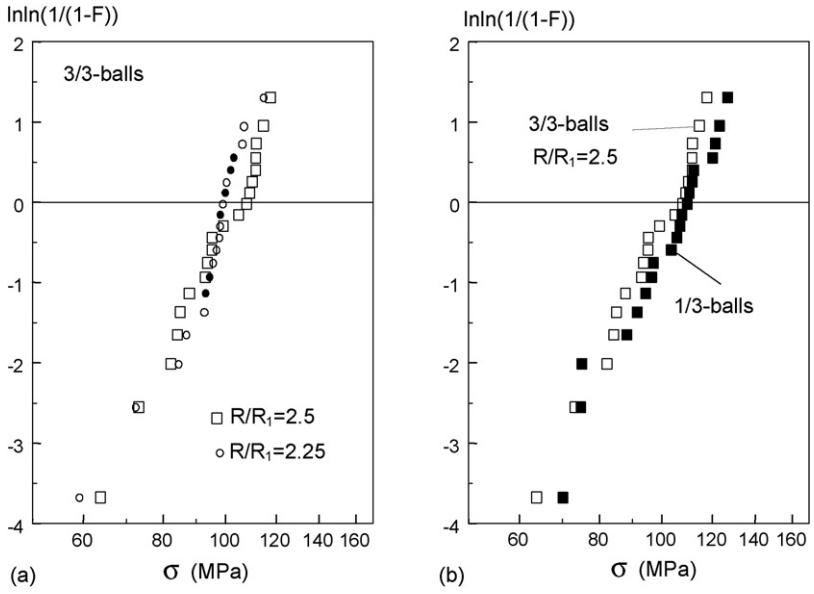

Fig. 18. Strength results of ground glass (a) 3-balls-on-3-balls tests with variable overhangs (open symbols: fractured in the centre region, solid symbols: fractured at the outer balls), (b) comparison between 3-balls-on-3-balls results with ball-on-3-balls strengths ($t = 4$ mm, $R = 45$ mm).

Table 1
Weibull parameters of ball-on-ball tests using ground glass ($t = 4$ mm, $R = 45$ mm)

Test	σ_0	m	m_{corr}
3/3-balls, $R_1 = 9$ mm, $R_2 = 20$ mm	99.8 [96.0; 103.9]	10.8 [7.4; 13.6]	10.0
3/3-balls, $R_1 = 9$ mm, $R_2 = 18$ mm	103.7 [98.6; 109.0]	8.5 [5.9; 10.8]	7.9
1/3-balls, $R_2 = 20$ mm	109.0 [103.3; 115.1]	7.9 [5.5; 10.0]	7.4

Table 2
Weibull parameters of ball-on-ball tests using polished glass ($t = 4$ mm, $R = 45$ mm)

Test	σ_0	m	m_{corr}
3/3-balls, $R_1 = 9$ mm, $R_2 = 18$ mm	157.4 [147.2; 168.5]	6.3 [4.3; 8.0]	5.9
1/3-balls, $R_2 = 20$mm	179.4 [162.6; 198.3]	4.3 [3.0; 5.4]	4.0

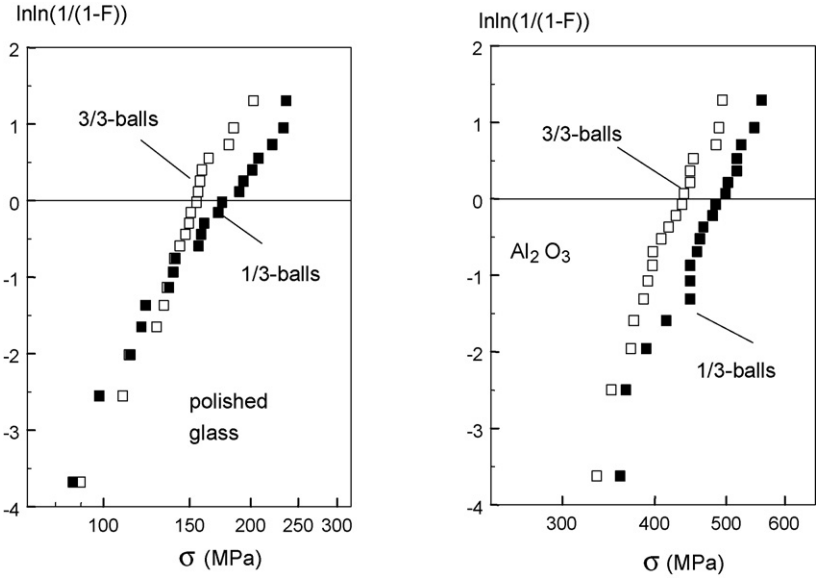

Fig. 19. Strength results of (a) polished glass ($R = 45$ mm, $t = 4$mm) and (b) alumina ($R = 45$ mm, $t = 2$ mm); 3-balls-on-3-balls tests with $R_1 = 9$ mm, $R_2 = 18$ mm, ball-on-3-balls tests with $R_2 = 20$ mm.

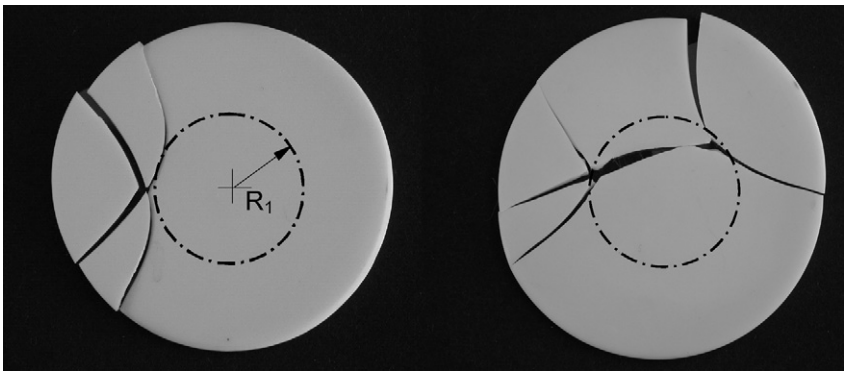

Fig. 20. Typically fractured alumina disks of 2 mm thickness (circles on which the inner spheres act are indicated by the dash-dotted lines).

Table 3
Weibull parameters of ball-on-ball tests using alumina ($t = 2$ mm, $R = 45$ mm)

Test	σ_0	m	m_{corr}
3/3-balls, $R_1 = 9$ mm, $R_2 = 18$ mm	437.9 [420.1; 456.8]	10.4 [7.1; 12.2]	9.7
1/3-balls, $R_2 = 20$ mm	491.0 [470.6; 513.0]	10.1 [6.9; 13.8]	9.4

Table 4
Estimation of the ratio of effective surfaces (assumption: identical biaxiality in both tests)

Test	$\sigma_{0,1B3B}/\sigma_{0,3B3B}$	m	$S_{eff,3B3B}/S_{eff,1B3B}$
Glass, ground (9/18)	1.051	8.2	1.5
Glass, ground (9/20)	1.092	9.7	2.35
Glass, polished	1.14	5.3	2.00
Alumina	1.121	10.25	3.22

6.2. Results on alumina

Strengths of alumina disks of 2 mm thickness are shown in Fig. 19b for the 3-balls-on-3-balls tests and ball-on-ball tests. The Weibull parameters determined with the Maximum Likelihood Procedure are compiled in Table 3.

Photos of typical fracture forms are shown in Fig. 20 for the alumina disks of 2 mm thickness. The dash-dotted lines indicate the circles on which the inner spheres act.

7. Discussion

The tests of glass specimens with variable overhangs showed that all specimens failed in the centre region if the overhang was chosen for

$$R - R_2 \geq t \tag{4}$$

This condition is therefore, recommended for practical use.

In all cases, the results of the 3-balls-on-3-balls tests are slightly lower than the strengths obtained from the ball-on-3-balls tests. The differences are 5.1% and 9.2% for the ground glass, 14% for the polished glass, and 12.1% for the alumina. The main reason for this tendency is assumed to be the influence of the different effective surfaces involved in the two types of tests. From the strength results, it has to be expected that the effective surface of the 3B3B tests is larger than that of the 1B3B tests.

Under the assumption of the multiaxiality being the same in both tests, the relation between the characteristic strengths σ_0 and effective surfaces S_{eff} is

$$\frac{\sigma_{3B3B}}{\sigma_{1B3B}} = \left(\frac{S_{eff,1B3B}}{S_{eff,3B3B}}\right)^{1/m} \tag{5}$$

with the Weibull exponent m. This exponent is different for the different tests. As can be seen from Tables 1–3, the 90% confidence intervals of the m-values overlap in all cases. For the evaluation of (5), we therefore, applied the average value as the common Weibull exponent. The resulting ratio of the effective surfaces obtained from the individual data of Tables 1–3 are compiled in Table 4. The average ratio of the effective surfaces is found to be about $S_{eff,3B3B}/S_{eff,1B3B} = 2.3$.

A ratio of roughly three had to be expected from the simplified assumption of the highly stressed zones opposite the (inner) loading spheres exclusively. The factor of three reflects the fact that the applied load is distributed over three spheres in the 3B3B test, compared with only one sphere in the 1B3B test.

As can be seen from Fig. 20, the failure starts predominantly near the inner loading spheres. This effect can be understood as the consequence of the fact that the effective surface is strongly concentrated in regions with high stresses. Under the assumption that the maximum principal stress σ_1 is responsible for failure, the effective surface can be expressed as

$$S_{eff} \propto \int_S \sigma_1^m \int_0^{2\pi} \sin\phi \, d\phi \, dS \tag{6}$$

where ϕ is the angle between a pre-existing (semi-circular) surface crack and the direction of σ_1. S is the geometric surface (for details see ref.[1]). From Eq. (6) it becomes clear that maximum contributions to the effective surface come from regions with high maximum principal stresses, i.e. from the regions opposite to the inner spheres. This concentration is very strong if the Weibull exponent m is large. For specimens with a low m-value, also the regions with lower stresses will contribute significantly to the effective surface.

In a separate study, the effective surfaces will be computed for the true (slightly different) multiaxiality of both tests, including

several additional failure criteria (normal stress, energy release rate, and Richard criterion, see ref.[36]). This effortful work is being carried out at the moment. The computations are performed on the basis of finite element stress analyses by use of the post-processor STAU.[37]

The extended surface of the 3B3B test with its reduced contact stress effect is an advantage compared to the 1B3B test. A disadvantage is the somewhat increased complexity in handling. Especially in the case of tests carried out on miniaturized specimens (with the typical space restrictions), a clear advantage of the 1B3B test is obvious. We therefore, consider to use the proposed test in cases where the ring-on-ring test is usually applied and specimen flatness and surface roughness are not of highest quality.

8. Summary

A test is proposed to determine the strength of ceramic disks under biaxial stress states. The load is applied by three symmetrically arranged spheres located on a small circle. Another three balls arranged on a larger circle are used for the support. Thus, clear loading conditions are guaranteed, similar to the ball-on-3-balls test.

For this test, the maximum principal stresses and the biaxiality are determined for a wide range of geometries by using the finite-element method. In first experiments, the strengths of glass and alumina were determined. Strengths in the 3-balls-on-3-balls arrangement were found to be slightly lower than strengths obtained from the ball-on-3-balls tests. The main reason for the differences may be the different effective surfaces.

Acknowledgment

The authors would like to thank the Deutsche Forschungsgemeinschaft DFG for financing parts of this work within the SFB 483.

References

1. Munz, D. and Fett, T., *Ceramics, mechanical properties, failure behaviour, materials selection*. Springer, Berlin, 1999.
2. Giovan, M. N. and Sines, G., Strength of a ceramic at high temperatures under biaxial and uniaxial tension. *J. Am. Ceram. Soc.*, 1981, **64**, 68–73.
3. German Standard DIN 52292, Teil 1: Prüfung von Glas und Glaskeramik, Bestimmung der Biegefestigkeit, Doppelring-Biegeversuch an plattenförmigen Proben mit kleinen Prüfflächen, Teil 2: Prüfung von Glas und Glaskeramik, Bestimmung der Biegefestigkeit, Doppelring-Biegeversuch an plattenförmigen Proben mit großen Prüfflächen.
4. Schmitt, W., Blank, K. and Schönbrunn, G., Experimentelle Spannungsanalyse zum Doppelringversuch. *Sprechsaal*, 1983, **116**, 397–405.
5. Fessler, H. and Fricker, D. C., A theoretical analysis of the ring-on-ring loading disc test. *J. Am. Ceram. Soc.*, 1984, **67**, 582–588.
6. Soltész, U., Richter, H. and Kienzler, R., *The concentric-ring-test and its application for determining the surface strength of ceramics, in high tech ceramics*. Elsevier Science Publishers, 1987, p. 149–58.
7. Marshall, D. B., An improved biaxial flexure test for ceramics. *Ceram. Bull.*, 1980, **59**, 551–553.
8. Quinn, G.D., NIST, Gaithersburg, MD, USA, personal communication.
9. Shetty, K. D., Rosenfield, A. R., McGuire, P. and Duckworth, W. H., Biaxial flexure test for ceramics. *Am. Ceram. Soc. Bull.*, 1980, **59**, 1193–1197.
10. Shetty, K. D., Rosenfield, A. R., McGuire, P., Bansal, G. K. and Duckworth, W. H., Biaxial fracture studies of a glass ceramic. *J. Am. Ceram. Soc.*, 1981, **64**, 1–4.
11. de With, G. and Wagemans, H. H. M., Ball-on-ring test revisited. *J. Am. Ceram. Soc.*, 1989, **72**, 1538–1541.
12. Godfrey, D. J. and John, S., In *Disc flexure tests for the evaluation of ceramic strength*, 1986, pp. 657–665.
13. Börger, A., Supancic, P. and Danzer, R., The ball on three balls test for strength testing of brittle discs: stress distribution in the disc. *J. Eur. Ceram. Soc.*, 2002, **22**, 1425–1436.
14. Börger, A., Supancic, P. and Danzer, R., The ball on three balls test for strength testing of brittle discs: Part II: analysis of possible errors in the strength determination. *J. Eur. Ceram. Soc.*, 2004, **24**, 2917–2928.
15. Danzer, R. *et al*., Methode und Vorrichtung zur Prüfung von Scheiben. Applied for Patent, A 738/2002-1, Austria, 2002.
16. Danzer, R. *et al.*, Ein einfacher Festigkeitsversuch für Scheiben aus spröden Werkstoffen. *Mat.-wiss. u. Werkstofftech.*, 2003, **34**, 490–498.
17. Carneiro, F. L. L. B. and Barcellos, A., *Résistance à la traction des bétons*. Instituto Nacional de Technologia, Rio de Janeiro, 1949.
18. Wright, P. J. F., Comments on an indirect tensile test on concrete cylinders. *Mag. Concrete Res.*, 1955, **7**, 87–96.
19. Shaw, M. C., Braiden, P. M. and De Salvo, G. J., The disk test for brittle materials. *Trans. ASME, J. Basic Eng. Ind.*, 1975, **97**, 77–87.
20. Hondros, G., The evaluation of Poisson's ratio and the modulus of materials of a low tensile resistance by the Brazilian (indirect tensile) test with particular reference to concrete. *Aust. J. Appl. Sci.*, 1959, **10**, 243–268.
21. Marion, R. H. and Johnstone, J. K., A parametric study of the diametral compression test for ceramics. *Am. Ceram. Soc. Bull.*, 1977, **56**, 998–1002.
22. Spriggs, R. M., Brissette, L. A. and Vasilos, T., Tensile strength of polycrystalline ceramics by the diametral compression test. *J. Mater. Res. Stand.*, 1964, **4**.
23. Szendi-Horvath, G., Fracture toughness determination of brittle materials using small to extremely small specimens. *Eng. Fract. Mech.*, 1980, **13**, 955–961.
24. Petroski, H. J. and Ojdrovic, R. P., The concrete cylinder: stress analysis and failure modes. *Int. J. Fract.*, 1987, **53**, 263–279.
25. Brückner-Foit, A., Fett, T., Munz, D. and Schirmer, K., Discrimination of multiaxiality criteria with the Brazilian disc test. *J. Eur. Ceram. Soc.*, 1997, **17**, 689–696.
26. Hasselman, D. P. H., Figures-of-merit for the thermal stress resistance of high-temperature brittle materials: a review. *Ceramurgia Int.*, 1978, **4**, 147.
27. Swain, M. V., R-curve behaviour and thermal shock resistance of ceramics. *J. Am. Ceram. Soc.*, 1990, **73**, 621–628.
28. Sato, S., Awaji, H., Kawamata, K., Kurumada, A. and Oku, T., Fracture criteria of reactor graphite under multiaxial stresses. *Nucl. Eng. Des.*, 1987, **103**, 291–300.
29. Ely, R. E., Strength of titania and aluminum silicate under combined stresses. *J. Am. Ceram. Soc.*, 1972, **55**, 347–350.
30. Adams, M. and Sines, G., Determination of biaxial compressive strength of a sintered alumina ceramic. *J. Am. Ceram. Soc.*, 1976, **59**, 300–304.
31. Boutman, L. J., Krishnakuman, S. M. and Mallick, P. K., Effects of combined stresses on fracture of alumina and graphite. *J. Am. Ceram. Soc.*, 1970, **53**, 649–654.
32. Fett, T., Oberacker, R., Vorrichtung zur Bestimmung der Festigkeit von keramischen Scheibenproben. Patentanmeldung, 2004.
33. Fett, T., Rizzi, G., A 3-balls-on-3-balls test for ceramic disks: A finite element study, Report FZKA 7052, Forschungszentrum Karlsruhe, Karlsruhe, 2004.
34. Thoman, D. R., Bain, L. J. and Antle, C. E., Inferences on the parameters of the Weibull distribution. *Technometrics*, 1969, **11**, 445.

35. European Standard ENV 843-5, Advanced monolithic ceramics – mechanical tests at room temperature – statistical analysis, European Committee for Standardisation, CEN TC184/WG3, London, UK.
36. Richard, H.A., Prediction of fracture of cracks subjected to combined tensile and shear loads (in German), VDI Research Report 631/85 (1985). Düsseldorf, Germany.
37. Heger, A., Brückner-Foit, A., Munz, D., STAU—ein Programm zur Berechnung der Ausfallwahrscheinlichkeit mehrachsig beanspruchter keramischer Komponenten als Post-Prozessor für Finite-Elemente-Programme, Internal Report 1991. Institute for Reliability and Failure Analysis, University of Karlsruhe, Germany.